Spin Backflow and ac Voltage Generation by Spin Pumping and the Inverse Spin Hall Effect

HuJun Jiao[1] and Gerrit E. W. Bauer[2,1]

[1]*Kavli Institute of NanoScience, Delft University of Technology, 2628 CJ Delft, The Netherlands*
[2]*Institute for Materials Research and WPI-AIMR, Tohoku University, Sendai 980-8577, Japan*

(Received 28 September 2012; published 23 May 2013)

The spin current pumped by a precessing ferromagnet into an adjacent normal metal has a constant polarization component parallel to the precession axis and a rotating one normal to the magnetization. The former is now routinely detected as a dc voltage induced by the inverse spin Hall effect (ISHE). Here we compute ac ISHE voltages much larger than the dc signals for various material combinations and discuss optimal conditions to observe the effect. The backflow of spin is shown to be essential to distill parameters from measured ISHE voltages for both dc and ac configurations.

DOI: 10.1103/PhysRevLett.110.217602 PACS numbers: 76.50.+g, 72.25.Mk, 73.40.−c

In magnetoelectronics the electronic spin degree of freedom creates new functionalities that lead to applications in information technologies such as sensors and memories [1]. Central to much excitement in this field is the spin Hall effect (SHE) [2–5], i.e., the spin current induced normal to an applied charge current in the presence of spin-orbit interaction, as discovered optically in semiconductors [6,7] and subsequently electrically in metals [8–10]. Recently magnetization reversal by the SHE induced spin transfer torque has been demonstrated [11,12]. The generation of a voltage by a spin current injected into a paramagnetic metal, the inverse spin Hall effect (ISHE), can be employed to detect the spin current due to spin pumping [13–15] by an adjacent ferromagnet under ferromagnetic resonance (FMR) conditions [8,16]. The ISHE has also been essential for the discovery of the spin Seebeck effect [17].

In recent experiments, dc voltages induced by the ISHE have been measured in many material combinations, thereby giving access to crucial parameters such as the spin Hall angle [18–20] and the spin mixing conductance [21], the material parameter determining, e.g., the effectiveness of interface spin-transfer torques [14]. For example, the magnitude and sign of the spin Hall angle has been determined for Permalloy (Py)|N bilayers for different normal metals N [18,19]. An approximate scaling relation for the spin pumping by numerous ferromagnets (F) has been discovered by comparing different F|Pt bilayers as a function of excitation power [21]. However, it is far from easy to derive quantitative information from ISHE experiments [22]. As reviewed by the Cornell Collaboration [23], several experimental pitfalls should be avoided. At FMR, the dc ISHE voltage is small, scaling quadratically with the cone angle of the precessing magnetization. An important correction is caused by the back diffusion ("backflow") of injected spins to the interface, which effectively reduces the spin current injection [14] and generates voltages normal to the interface [24,25]. This backflow has often been neglected in interpreting spin-pumping experiments, assuming that Pt, the metal of choice, can be treated like a perfect spin sink.

The spin current injected by FMR into a normal metal consists of a dc component along the z axis parallel to the effective field and an ac component normal to it, i.e., in the xy plane (see Fig. 1). In this Letter we analyze both ac and dc ISHE voltages by time-dependent spin diffusion theory, where the former is generated between the edges of the sample along the z direction, i.e., for a different magnetic or sample configuration than used for dc signal detection. For small precession angles we find the ac ISHE voltage to be orders of magnitude larger than the dc signal. The backflow of spins modifies also the dc voltage even for small spin-flip diffusion lengths, requiring a reappraisal of published parameters.

A normal metal in contact with a ferromagnet under FMR as shown in Fig. 1 can be interpreted as a spin battery [26]. When the ferromagnetic film is thicker than its transverse spin-coherence length (a few monolayers), the adiabatically pumped spin current reads [13–15,26]

$$\mathbf{I}_s^p = \frac{\hbar}{4\pi}\left(\mathrm{Re}g^{\uparrow\downarrow}\mathbf{m}\times\frac{d\mathbf{m}}{dt} + \mathrm{Im}g^{\uparrow\downarrow}\frac{d\mathbf{m}}{dt}\right), \tag{1}$$

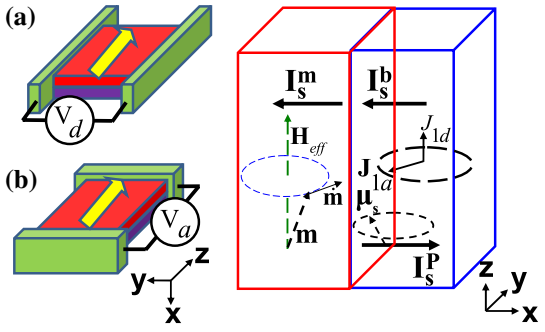

FIG. 1 (color online). Schematic spin battery operated by FMR, for the measurement configurations (a) and (b). The ac (dc) voltage drops along the z (y) direction. The right panel introduces the parameters of the model. The effective field $\mathbf{H}_{\mathrm{eff}}$ is the sum of the external field $\mathbf{H}_{\mathrm{ex}}$ and the uniaxial field $\mathbf{H}_{\mathrm{un}}$, $\mathbf{H}_{\mathrm{ex}}$, and $\mathbf{H}_{\mathrm{un}}$ point along the z axis. The dc component $J_{1d}(j_{1s}^z)\mathbf{e}_z$ and ac component $\mathbf{J}_{1a}(\mathbf{j}_{1s}^a)$ constitute the spin current $\mathbf{j}_{1s}$.

where $\mathbf{m}$ is the unit vector of the magnetization direction and $g^{\uparrow\downarrow}$ is the (dimensionless) complex spin mixing conductance [27]. The pumping spin current creates a spin accumulation in N that induces a diffusion backflow of spins into F:

$$\mathbf{I}_s^b = \frac{g}{8\pi}[2p(\mu_0^F - \mu_0^N) + \mu_s^F - \mathbf{m}\cdot\boldsymbol{\mu}_s^N]\mathbf{m} - \frac{\mathrm{Re}g^{\uparrow\downarrow}}{4\pi}\mathbf{m}\times(\boldsymbol{\mu}_s^N\times\mathbf{m}) + \frac{\mathrm{Im}g^{\uparrow\downarrow}}{4\pi}\mathbf{m}\times\boldsymbol{\mu}_s^N, \quad (2)$$

where μ_0^N, $\boldsymbol{\mu}_s^N$ in N and μ_0^F, $\mu_s^F\mathbf{m}$ in F are the charge and spin accumulations at the interface. The total conductance $g = g^{\uparrow\uparrow} + g^{\downarrow\downarrow}$ is the sum of spin-up and spin-down interface conductances, and $p = (g^{\uparrow\uparrow} - g^{\downarrow\downarrow})/(g^{\uparrow\uparrow} + g^{\downarrow\downarrow})$ is the conductance spin polarization. The magnetization determined by the Landau-Lifshitz-Gilbert equation is assumed to precess with constant cone angle θ around the z axis, whose magnitude is governed by the rf radiation intensity. The spin accumulation in N obeys the spin-diffusion equation [28]

$$\frac{\partial\boldsymbol{\mu}_s^N(\mathbf{r},t)}{\partial t} = \gamma_N\mathbf{H}_{\mathrm{ex}}\times\boldsymbol{\mu}_s^N + D_N\frac{\partial^2\boldsymbol{\mu}_s^N}{\partial x^2} - \frac{\boldsymbol{\mu}_s^N}{\tau_{\mathrm{sf}}^N}, \quad (3)$$

where γ_N is the gyromagnetic ratio, D_N is the diffusion constant, and τ_{sf}^N is the spin-flip relaxation time, all in N. The spin current $\mathbf{I}_s = \mathbf{I}_s^p + \mathbf{I}_s^b$ is continuous at the $N|F$ interface and vanishes at the outer boundary $x = d_N$. In position-frequency space the exact solution for the spatio-temporal dependence of the spin accumulation reads

$$\boldsymbol{\mu}_s^N(x,\omega) = \sum_{i=1}^{3}\vec{v}_i\frac{\cosh[\kappa_i(x-d_N)]}{\sinh[\kappa_i d_N]}\frac{2j_{is}(x=0,\omega)}{\hbar\nu D_N\kappa_i}. \quad (4)$$

$\kappa_1^2(\omega) = (1 + i\omega\tau_{\mathrm{sf}}^N)/(\lambda_{\mathrm{sd}}^N)^2$, $\kappa_{2,3}^2(\omega) = \kappa_1^2(\omega) \pm iC$, $C = -\gamma_N H_{\mathrm{ex}}/D_N$, and $\lambda_{\mathrm{sd}}^N = \sqrt{D_N\tau_{\mathrm{sf}}^N}$. $j_{1s} = I_s^z/A$ and $j_{(2,3)s} = (I_s^x \pm iI_s^y)/(\sqrt{2}A)$ are spin current densities, where ν is the one-spin density of state and A is the interface area. The eigenvectors associated with $\kappa_i^2(\omega)$ $(i = 1, 2, 3)$ are, respectively, $\vec{v}_1 = (0\ 0\ 1)$, $\vec{v}_2 = (1\ \ -i\ 0)/\sqrt{2}$, $\vec{v}_3 = (1\ i\ 0)/\sqrt{2}$. In the position-time domain

$$\mathbf{j}_{1s}(x,t) = -\frac{\hbar\nu D_N}{2}\frac{\partial\boldsymbol{\mu}_s^N(x,t)}{\partial x} = j_{1s}^z(x)\mathbf{e}_z + \mathbf{j}_{1s}^a(x,t), \quad (5)$$

with

$$j_{1s}^z(x)\mathbf{e}_z = \frac{\sinh[\kappa_1(0)(d_N - x)]}{\sinh[\kappa_1(0)d_N]}j_{1s}^z(0)\mathbf{e}_z, \quad (6)$$

$$\mathbf{j}_{1s}^a(x) = 2\,\mathrm{Re}\left\{\frac{\sinh[\kappa_2(\omega)(d_N - x)]}{\sinh[\kappa_2(\omega)d_N]}\mathbf{j}_{1s}^a(0)e^{i\omega t}\right\}. \quad (7)$$

The analytic expressions for $j_{1s}^z(0)$ and $\mathbf{j}_{1s}^a(0)$, the dc and ac components of the spin current at the N side of the interface, respectively, are given in the Supplemental Material [29].

The longitudinal component of the spin accumulation can penetrate F, leading to a spin accumulation $\mathbf{m}(t)\mu_s^F$. $\mu_s^F = \mu_\uparrow^F - \mu_\downarrow^F$ that satisfies the spin-diffusion equation [28]

$$\frac{\partial^2\mu_s^F(x)}{\partial x^2} = \frac{\mu_s^F(x)}{(\lambda_{\mathrm{sd}}^F)^2}, \quad (8)$$

where λ_{sd}^F is the spin-flip diffusion length in the ferromagnet. In an open circuit the dc charge current vanishes and we obtain

$$\mu_s^F(x) = \frac{\cosh[(d_F + x)/\lambda_{\mathrm{sd}}^F]\tilde{g}}{[g_F\tanh[d_F/\lambda_{\mathrm{sd}}^F] + \tilde{g}]\cosh(d_F/\lambda_{\mathrm{sd}}^F)}\mathbf{m}\cdot\boldsymbol{\mu}_s^N, \quad (9)$$

where $g_F = 4hA\sigma_\uparrow\sigma_\downarrow/[e^2\lambda_{\mathrm{sd}}^F(\sigma_\uparrow + \sigma_\downarrow)]$ and $\tilde{g} = (1 - p^2)g$. Here, $\sigma_{\uparrow(\downarrow)}$ is the conductivity of spin-up (spin-down) electrons in F. The spin current density in F reads

$$\mathbf{j}_{2s}(x) = \frac{\sinh[(d_F + x)/\lambda_{\mathrm{sd}}^F]}{\sinh(d_F/\lambda_{\mathrm{sd}}^F)}\mathbf{j}_{2s}(0), \quad (10)$$

with

$$\mathbf{j}_{2s}(0) = -\frac{1}{8\pi}\frac{\tilde{g}g_F\tanh[d_F/\lambda_{\mathrm{sd}}^F]}{\tilde{g} + g_F\tanh[d_F/\lambda_{\mathrm{sd}}^F]}(\mathbf{m}\cdot\boldsymbol{\mu}_s^N)\mathbf{m} \quad (11)$$

at the interface. When spin flip in F is negligible, $\lambda_{\mathrm{sd}}^F \gg d_F$, $\mu_s^F(0) = \mathbf{m}\cdot\boldsymbol{\mu}_s^N$ and the spin current in F vanishes. The transverse backflow spin current modifies the magnetization dynamics by contributing a three-component transfer torque that (i) reduces the interface Gilbert damping due to spin pumping, (ii) modulates the gyromagnetic ratio, and (iii) adds an effective magnetic field. For the system parameters considered below the last two terms are too small to significantly affect the magnetization dynamics, however.

The ISHE generates a charge current $\mathbf{j}_c$ transverse to an applied spin current due to the spin-orbit interaction. With the spin current direction along $\mathbf{e}_x$ [8,16,18–21],

$$\mathbf{j}_c(x) = \alpha_{N/F}(2e/\hbar)\mathbf{e}_x\times\mathbf{j}_s(x), \quad (12)$$

where α_N is the spin Hall angle in N and $\alpha_F = (\alpha_{F\uparrow} + \alpha_{F\downarrow})/2$ is that in F, where $\alpha_{F\xi} = \sigma_{\mathrm{AH}\xi}/\sigma_\xi$ $(\xi = \uparrow, \downarrow)$ and $\sigma_{(\mathrm{AH})\xi}$ is the spin-polarized (anomalous Hall) conductivity. As shown in Fig. 1(a), a dc electric field $E_y\mathbf{e}_y$ is generated along the y direction; similarly, an ac field $E_z(t)\mathbf{e}_z$ along the z direction is shown in Fig. 1(b). Disregarding parasitic impedances and in the steady state, we obtain for the ac contribution along z

$$E_z(t) = \frac{4e/\hbar}{\sigma_N d_N + \sigma_F d_F}\mathrm{Re}\left(\frac{\alpha_N j_{1s}^y(0)}{\kappa_2(\omega)}\tanh\frac{d_N\kappa_2(\omega)}{2} + \alpha_F j_{2s}^y(0)\lambda_{\mathrm{sd}}^F\tanh\frac{d_N}{2\lambda_{\mathrm{sd}}^N}\right), \quad (13)$$

while the dc electric field along y reads

$$E_y = \frac{2e/\hbar}{\sigma_N d_N + \sigma_F d_F}\left[j_{1s}^z(0)\alpha_N\lambda_{\mathrm{sd}}^N\tanh\frac{d_N}{2\lambda_{\mathrm{sd}}^N} + j_{2s}^z(0)\alpha_F\lambda_{\mathrm{sd}}^F\tanh\frac{d_F}{2\lambda_{\mathrm{sd}}^F}\right]. \quad (14)$$

TABLE I. Parameters for selected bilayer systems used to compute dc and ac ISHE electric fields induced by spin pumping under FMR.

Material	$\nu_{\mathrm{DOS}}(2\nu)$ [10^{47} J^{-1} m^{-3}]	$\sigma_{N,F,H}$ [10^6 Ω^{-1} m^{-1}]	$\lambda_{\mathrm{sd}}^{N,F}$ [nm]	$\alpha_{N,F}$ [10^{-2}]	$g_N^{sh}, g/A$ [10^{19} m^{-2}]
Al	1.5 [33]	11 [34]	350 [34]	0.01 [9]	3.6
Ta	4.3 [33]	0.53 [12]	2.7 [35]	−15 [12]	2.5
Au	1.1 [33]	25.2 [18]	35 [18]	0.35 [18]	1.2
Pd	10.0 [33]	4.0 [18]	15 [18]	0.64 [18]	1.6
Pt	9.1 [33]	5 [23]	1.5 [23]	7 [23]	1.8
Py	$q = 0.7$	1.5	5 [36]	7.6	$p_H = 0.5$
	Py|NM	YIG|Au		YIG|Pt	p
$\mathrm{Re}g^{\uparrow\downarrow}/A$	$2g_N^{\mathrm{sh}}/A$	0.66 [37]		2.3 [32]	0.4

$q \equiv (\sigma_\uparrow - \sigma_\downarrow)/\sigma_F \cdot p_H \equiv (\sigma_{\mathrm{AH}\uparrow} - \sigma_{\mathrm{AH}\downarrow})/\sigma_H \cdot \sigma_H = 0.09$ [38]. Schep corrections [39,40] are included in $\mathrm{Re}g^{\uparrow\downarrow}/A$.

These equations are our main result. In Eqs. (13) and (14) the first terms come from the ISHE in N, and the second terms are due to the anomalous Hall effect in F. $j_{1s}^z(0)$ and $j_{1s}^y(0)$ are the dc(z) and ac(y) components of the spin current at the $N(1)$ side of the interface, respectively; $j_{2s}^z(0)$ and $j_{2s}^y(0)$ are the counterparts at the $F(2)$ side of the interface. In the following we disregard $\mathrm{Im}g^{\uparrow\downarrow}$ which is small for the interfaces considered below [30–32]. When backflow is disregarded, the ac signal reduces to

$$\frac{E_z^{NB}(t)}{\cos(\omega t + \delta)} = \frac{e\alpha_N f \sin\theta\cos\theta}{\sigma_N d_N + \sigma_F d_F}\frac{\mathrm{Re}g^{\uparrow\downarrow}}{A}\left|\frac{\tanh[\kappa_2(\omega)d_N/2]}{\kappa_2(\omega)}\right|, \tag{15}$$

where $\delta = \delta_0 + \mathrm{Arg}\{\tanh[\kappa_2(\omega)d_N/2]/\kappa_2(\omega)\}$, with $\delta_0 = -\pi$ for $\alpha_N > 0$ and 0 for $\alpha_N < 0$, is the phase shift relative to the rf excitation field $\cos(\omega t)\mathbf{e}_y$. We also recover the dc relation [18,19]

$$E_y^{NB} = \frac{e\alpha_N f \sin^2\theta}{\sigma_N d_N + \sigma_F d_F}\frac{\mathrm{Re}g^{\uparrow\downarrow}}{A}\lambda_{\mathrm{sd}}^N \tanh\frac{d_N}{2\lambda_{\mathrm{sd}}^N}. \tag{16}$$

The spin-pumping induced spin accumulation is governed by two length scales λ_{sd}^N and the transverse spin dephasing length $\lambda_c = \sqrt{D_N/\omega}$ [14], which determine the decay rates of the dc and ac components in N, respectively. From $\omega \ll 1/\tau_{\mathrm{sf}}^N$ follows $\lambda_{\mathrm{sd}}^N \ll \lambda_c$. This is the case when $\omega\tau_{\mathrm{sf}}^N \simeq 0.2(f/10\ \mathrm{GHz})(\tau_{\mathrm{sf}}^N/3\ \mathrm{ps}) \ll 1$. In Pt(Ta) $\omega\tau_{\mathrm{sf}}^N = 1(15) \times 10^{-3}$ at $f = 15.5$ GHz with $\tau_{\mathrm{sf}}^{\mathrm{Pt(Ta)}} = 0.01(0.15)$ ps as calculated from the data in Table I. So in the FMR frequency region the condition $\omega\tau_{\mathrm{sf}}^N \ll 1$ is fulfilled for elemental metals with a large ISHE. In that limit the contribution from the anomalous Hall effect in a ferromagnet such as Py is found to be negligible. Previous expressions for the dc spin accumulation [14] and voltages [41,42] agree with the present results in that limit. Note that this condition does not hold for metals with long spin-flip times, for example, single crystal Al.

In Fig. 2, we plot the dc electric fields including the backflow of spin as a function of spin Hall angle α_N and spin diffusion length λ_{sd}^N (noting that the results are very insensitive to changes in λ_{sd}^F and α_F). The strong correlation between these two parameters especially for YIG|Pt is evident. Nevertheless, we can narrow them down when the Gilbert damping interface enhancement is measured simultaneously [41]. The spin-mixing conductance $(\mathrm{Re}g_{\mathrm{eff}}^{\uparrow\downarrow}/A)^{-1} = (\mathrm{Re}g^{\uparrow\downarrow}/A)^{-1} + \Gamma^{-1} = 3 \times 10^{19}\ \mathrm{m}^{-2}$ where $\Gamma = (h/e^2)\sigma_N/(2\lambda_{\mathrm{sd}}^N)$ for $d_N \to \infty$ can be obtained from the Gilbert damping constant $\zeta_{\mathrm{eff}} = \zeta_0 + (\gamma_F\hbar)/(4\pi M_s d_F)\mathrm{Re}g_{\mathrm{eff}}^{\uparrow\downarrow}/A$ [14]. The conductivities are parametrized as $\sigma_{N(F)} = 4.1(3.5) \times (1 - e^{-d_{N(F)}/29.6(9.8)}) \times 10^6\ \Omega^{-1}\,\mathrm{m}^{-1}$ to fit the experiments (cf. the Supplemental Material [29]) [43]. Since $\mathrm{Re}g^{\uparrow\downarrow} > 0$ the experiments provide the important constraint that $\lambda_{\mathrm{sd}}^N < 1.8$ nm, which is not consistent with larger values in use for this parameter. The constraint that the spin-flip scattering relaxation time should be larger than the scattering lifetime leads to $\lambda_{\mathrm{sd}}^N > 0.9$ nm based on the free-electron model for N [14,41]. In Fig. 3 we plot the computed and the measured spin Hall voltages as a function of the layer thicknesses for optimized parameter combinations with and without backflow. The largest ISHE voltages are generated for $d_N \simeq 10\lambda_{\mathrm{sd}}^N(12\ \mathrm{nm})$ (see below) [20,41,42]. Since the above estimates favor $\lambda_{\mathrm{sd}}^N \approx 1.3$ nm, we estimate the Hall angle $\alpha_{\mathrm{Pt}} \approx 0.12$ from the spin-pumping experiments [41] and consistency arguments alone. These parameters differ from those reported [20,41], illustrating the importance of taking into account the experimental constraint on λ_{sd}^N provided by the increased Gilbert damping. The spin diffusion length extracted from the ISHE experiment also differs

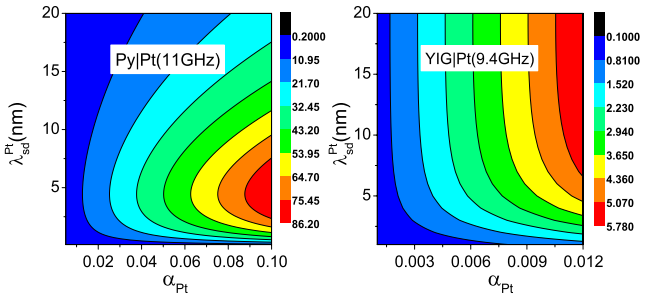

FIG. 2 (color online). The calculated dc ISHE electric fields (in units of μV/mm) including spin backflow as a function of the spin Hall angle and the spin-flip diffusion length based on the parameters in Table I.

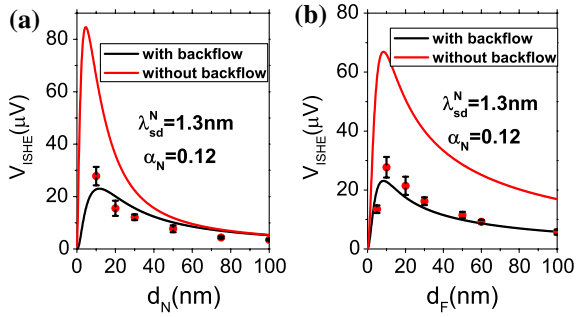

FIG. 3 (color online). Theoretical and experimental [41] dc ISHE voltages in Pt|Py bilayers as a function of Pt thickness (a) and Py thickness (b) using parameters given in Ref. [41].

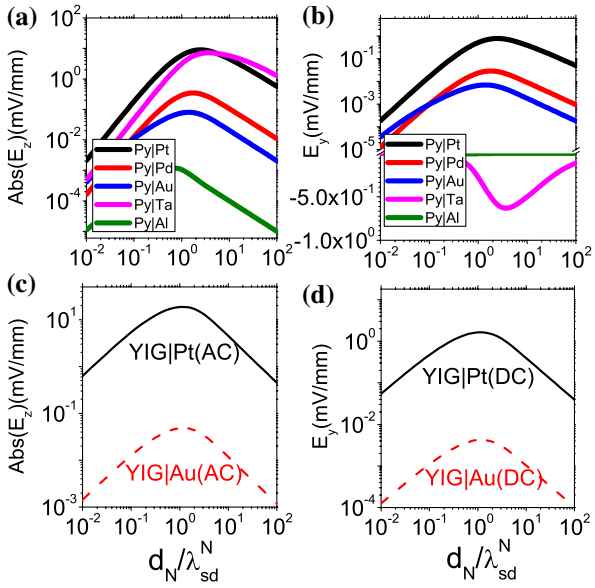

FIG. 4 (color online). The ac and dc electric fields as a function of d_N for Py|N and YIG|N for a fixed FMR frequency of 15.5 GHz. Here, the precession angle is 5° and $d_F = 15$ nm. Other parameters are taken from Table I.

from that from the low-temperature giant magnetoresistance (GMR) measurements [44], which is mainly caused by the large discrepancy in the electrical conductivities [23]. Utilizing the relation between spin relaxation and conductivity implied by the Elliot-Yafet mechanism [45], we can extrapolate the GMR measurements from low to room temperature, leading to a spin diffusion length $\lambda_{\rm sd}^N \approx$ 2.4 nm, which is about two times larger than the spin-pumping result above.

In Fig. 4 we turn to the ac ISHE by comparing its dependence on the normal metal thickness with the dc counterpart for a precession angle of 5° for Py|N (N = Au, Ta, Pd, Pt, and Al) and YIG|N (N = Pt, Au) bilayers. Both ISHE fields are maximized for $d_N \gtrsim 2\lambda_{\rm sd}^N$ since both ac and dc signals are affected by both the spin current reach and the effective resistance. Increasing d_N from zero, the total spin current initially increases exponentially because of reduction of the backflow of spins back into F. When the thickness increases far beyond $2\lambda_{\rm sd}^N$, the emf generated by the ISHE close to the interface is short circuited by the inactive part of N that leads to an algebraic decrease of the voltage for larger d_N. A systematic experimental study of the dc ISHE and Gilbert damping as a function of $d_N \in [2, 10]\lambda_{\rm sd}^N$ should help to understand the backflow and lead to more accurate parameter determinations, including $\lambda_{\rm sd}^N$. The ac voltage is proportional to the precession angle (square root of the rf excitation power), in contrast to the linear relation between dc voltage and excitation power [18,19,46]. Furthermore, the ratio of the ac to dc field modulus is much larger than unity for the intensities typical for FMR experiments. This ratio is close to a universal function as long as the anomalous Hall effect does not play a role (always the case for magnetic insulators) approaching the scaling function $C(\omega)\cot\theta$, where $C(\omega)$ is material dependent. When $\omega \ll 1/\tau_{\rm sf}^N$, $C(\omega) \simeq 1$, which is the case for Pt, Pd, Au, and Ta. We furthermore note that for constant precession angles, the voltages increase with the FMR frequency due to the increased spin pumping $\sim|\dot{\mathbf{m}}|$. When on the other hand the rf intensity is kept constant with frequency, the precession angle is inversely proportional to the FMR frequency and increasing ω leads to decreasing dc voltage, while the ac voltage remains roughly constant. We find that the anomalous Hall effect in Py caused by the backflow of spins into the ferromagnet is negligible unless the ISHE in the normal metal is very small, as, e.g., in single crystal Al, in which the phase of the ac fields becomes interesting (see Fig. S3 in the Supplemental Material [29]).

Current-induced magnetization reversal in ferromagnet-normal metal bilayers [11,12] has attracted much attention. Whether the current-induced transfer torque is caused by the SHE in the normal metal or spin orbit interaction in the ferromagnet [47] or at the interface [48] is still a matter of controversy. While the present study does not directly contribute to these issues, it should help the quest to find consistent models for this important material class.

In summary, we present a theory of the dynamics of ISHE detection of spin pumping, explicitly including the back diffusion of spins into the ferromagnet. We predict the generation of an ac voltage along the effective magnetic field in $F|N$ bilayers under FMR. We predict magnitudes and phase shifts of the ac voltages for Py|N and YIG|N. From the analysis of published experiments, we predict that the spin Hall angle in Pt is 0.12. If the ISHE signal can be separated from parasitic voltages at the resonance frequency, the much larger ac signals could be an attractive alternative to detect spin currents.

This work was supported by the FOM Foundation, EU-ICT-7 "MACALO," the ICC-IMR, and DFG Priority Programme 1538 "Spin-Caloric Transport." We thank Professors Can-Ming Hu, Bechara Muniz, Sergio Rezende, and MinZhong Wu for their comments on the first version of the manuscript and Mathias A. Weiler for pointing out a missing factor of 2.

[1] S. D. Bader and S. S. P. Parkin, Annu. Rev. Condens. Matter Phys. **1**, 71 (2010).
[2] J. E. Hirsch, Phys. Rev. Lett. **83**, 1834 (1999).
[3] S. Zhang, Phys. Rev. Lett. **85**, 393 (2000).
[4] S. Murakami, N. Nagaosa, and S. C. Zhang, Science **301**, 1348 (2003).
[5] J. Sinova, D. Culcer, Q. Niu, N. A. Sinitsyn, T. Jungwirth, and A. H. MacDonald, Phys. Rev. Lett. **92**, 126603 (2004).
[6] Y. K. Kato, R. C. Myers, A. C. Gossard, and D. D. Awschalom, Science **306**, 1910 (2004).
[7] J. Wunderlich, B. Kaestner, J. Sinova, and T. Jungwirth, Phys. Rev. Lett. **94**, 047204 (2005).
[8] E. Saitoh, M. Ueda, H. Miyajima, and G. Tatara, Appl. Phys. Lett. **88**, 182509 (2006).
[9] S. O. Valenzuela and M. Tinkham, Nature (London) **442**, 176 (2006).
[10] T. Kimura, Y. Otani, T. Sato, S. Takahashi, and S. Maekawa, Phys. Rev. Lett. **98**, 156601 (2007).
[11] I. M. Miron, K. Garello, G. Gaudin, P. J. Zermatten, M. V. Costache, S. Auffret, S. Bandiera, B. Rodmacq, A. Schuhl, and P. Gambardella, Nature (London) **476**, 189 (2011).
[12] L. Liu, C.-F. Pai, Y. Li, H.-W. Tseng, D. C. Ralph, and R. A. Buhrman, Science **336**, 555 (2012).
[13] Y. Tserkovnyak, A. Brataas, and G. E. W. Bauer, Phys. Rev. Lett. **88**, 117601 (2002).
[14] Y. Tserkovnyak, A. Brataas, G. E. W. Bauer, and B. Halperin, Rev. Mod. Phys. **77**, 1375 (2005).
[15] F. S. M. Guimarães, A. T. Costa, R. B. Muniz, and D. L. Mills, Phys. Rev. B **84**, 054403 (2011).
[16] A. Azevedo, L. H. Vilela Leão, R. L. Rodriguez-Suarez, A. B. Oliveira, and S. M. Rezende, J. Appl. Phys. **97**, 10C715 (2005).
[17] K. Uchida, S. Takahashi, K. Harii, J. Ieda, W. Koshibae, K. Ando, S. Maekawa, and E. Saitoh, Nature (London) **455**, 778 (2008).
[18] O. Mosendz, V. Vlaminck, J. E. Pearson, F. Y. Fradin, G. E. W. Bauer, S. D. Bader, and A. Hoffmann, Phys. Rev. B **82**, 214403 (2010).
[19] O. Mosendz, J. E. Pearson, F. Y. Fradin, G. E. W. Bauer, S. D. Bader, and A. Hoffmann, Phys. Rev. Lett. **104**, 046601 (2010).
[20] A. Azevedo, L. H. Vilela-Leão, R. L. Rodríguez-Suárez, A. F. Lacerda Santos, and S. M. Rezende, Phys. Rev. B **83**, 144402 (2011).
[21] F. D. Czeschka, L. Dreher, M. S. Brandt, M. Weiler, M. Althammer, I.-M. Imort, G. Reiss, A. Thomas, W. Schoch, W. Limmer, H. Huebl, R. Gross, and S. T. B. Goennenwein, Phys. Rev. Lett. **107**, 046601 (2011).
[22] Z. Feng, J. Hu, L. Sun, B. You, D. Wu, J. Du, W. Zhang, A. Hu, Y. Yang, D. M. Tang, B. S. Zhang, and H. F. Ding, Phys. Rev. B **85**, 214423 (2012).
[23] L. Liu, R. A. Buhrman, and D. C. Ralph, arXiv:1111.3702.
[24] X. Wang, G. E. W. Bauer, B. J. van Wees, A. Brataas, and Y. Tserkovnyak, Phys. Rev. Lett. **97**, 216602 (2006).
[25] M. V. Costache, M. Sladkov, S. M. Watts, C. H. van der Wal, and B. J. van Wees, Phys. Rev. Lett. **97**, 216603 (2006).
[26] A. Brataas, Y. Tserkovnyak, G. E. W. Bauer, and B. I. Halperin, Phys. Rev. B **66**, 060404(R) (2002).
[27] A. Brataas, Yu. V. Nazarov, and G. E. W. Bauer, Phys. Rev. Lett. **84**, 2481 (2000); Eur. Phys. J. B **22**, 99 (2001).
[28] M. Johnson and R. H. Silsbee, Phys. Rev. B **37**, 5312 (1988).
[29] See Supplemental Material at http://link.aps.org/supplemental/10.1103/PhysRevLett.110.217602 for detailed information for the spin current, parametrized electrical conductivities, and phase shifts.
[30] K. Xia, P. J. Kelly, G. E. W. Bauer, A. Brataas, and I. Turek, Phys. Rev. B **65**, 220401(R) (2002).
[31] M. Zwierzycki, Y. Tserkovnyak, P. J. Kelly, A. Brataas, and G. E. W. Bauer, Phys. Rev. B **71**, 064420 (2005).
[32] X. Jia, K. Liu, K. Xia, and G. E. W. Bauer, Europhys. Lett. **96**, 17005 (2011).
[33] D. A. Papaconstantopoulos, *Handbook of the Band Structure of Elemental Solids* (Plenum, New York, 1986).
[34] F. J. Jedema, H. B. Heersche, A. T. Filip, J. J. A. Baselmans, and B. J. van Wees, Nature (London) **416**, 713 (2002); M. Zaffalon and B. J. van Wees, Phys. Rev. Lett. **91**, 186601 (2003).
[35] M. Morota, Y. Niimi, K. Ohnishi, D. H. Wei, T. Tanaka, H. Kontani, T. Kimura, and Y. Otani, Phys. Rev. B **83**, 174405 (2011).
[36] J. Bass and W. P. Pratt, Jr., J. Magn. Magn. Mater. **200**, 274 (1999).
[37] C. Burrowes, B. Heinrich, B. Kardasz, E. A. Montoya, E. Girt, Y. Sun, Y. Y. Song, and M. Wu, Appl. Phys. Lett. **100**, 092403 (2012).
[38] T. Miyasato, N. Abe, T. Fujii, A. Asamitsu, S. Onoda, Y. Onose, N. Nagaosa, and Y. Tokura, Phys. Rev. Lett. **99**, 086602 (2007).
[39] K. M. Schep, J. B. A. N. van Hoof, P. J. Kelly, G. E. W. Bauer, and J. E. Inglesfield, Phys. Rev. B **56**, 10805 (1997).
[40] G. E. W. Bauer, K. M. Schep, K. Xia, and P. J. Kelly, J. Phys. D **35**, 2410 (2002).
[41] H. Nakayama, K. Ando, K. Harii, T. Yoshino, R. Takahashi, Y. Kajiwara, K. Uchida, Y. Fujikawa, and E. Saitoh, Phys. Rev. B **85**, 144408 (2012).
[42] V. Castel, N. Vlietstra, J. B. Youssef, and B. J. van Wees, Appl. Phys. Lett. **101**, 132414 (2012).
[43] The use of a thickness dependent conductivity with constant spin-flip diffusion length implies a thickness dependent spin-flip scattering time. Assumption of a constant spin-flip scattering time in N would then lead to spin-flip diffusion lengths that decrease with film thickness.
[44] H. Kurt, R. Loloee, K. Eid, W. P. Pratt, and J. Bass, Appl. Phys. Lett. **81**, 4787 (2002).
[45] J. Fabian and S. Das Sarma, J. Vac. Sci. Technol. B **17**, 1708 (1999).
[46] K. Ando, S. Takahashi, J. Ieda, Y. Kajiwara, H. Nakayama, T. Yoshino, K. Harii, Y. Fujikawa, M. Matsuo, S. Maekawa, and E. Saitoh, J. Appl. Phys. **109**, 103913 (2011).
[47] A. Manchon and S. Zhang, Phys. Rev. B **79**, 094422 (2009).
[48] A. Thiaville, S. Rohart, É. Jué, V. Cros, and A. Fert, Europhys. Lett. **100**, 57002 (2012).